Modern Pathology (2020) 33:1360–1368
https://doi.org/10.1038/s41379-020-0493-4

ARTICLE

Recurrent novel *THBS1-ADGRF5* gene fusion in a new tumor subtype "Acral FibroChondroMyxoid Tumors"

Corinne Bouvier[1] · François Le Loarer[2] · Nicolas Macagno[1] · Sébastien Aubert[3] · Virginie Audard[4] · Damien Geneste[5] · Anne Gomez-Brouchet[6] · Jean-Marc Guinebretière[7] · Frédérique Larousserie[4] · Daniel Pissaloux[8] · Béatrice Marie[9] · Franck Tirode[8] · Jessica Baud[10] · Gonzague De Pinieux[11]

Received: 7 November 2019 / Revised: 16 January 2020 / Accepted: 16 January 2020 / Published online: 11 February 2020

Abstract

Acral soft tissue tumors are common neoplasms, a subset of which pose a diagnostic challenge. We report 10 cases of a previously unrecognized acral benign soft tissue tumor. These tumors arose on the fingers and toes and involved bone in half of cases. Histologically, the tumors were lobulated and displayed an abundant stroma made of variable fibrous, chondroid and myxoid material reminiscent of cartilaginous or myoepithelial differentiation. Tumor cells harbored small round to reniform nuclei with clear chromatin and inconspicuous nucleoli along with scant eosinophilic cytoplasm. The cells were mostly arranged haphazardly in the stroma but also in small clusters. No mitotic activity was detected. No specific feature was identified in recurrent cases. By immunohistochemistry, the cells consistently stained for CD34 (10/10), ERG (9/10), and SOX9 (7/10). Whole RNA sequencing identified a previously undescribed recurrent in frame *THBS1-ADGRF5* gene fusion in all cases. The transcript was confirmed by RT-PCR and was not found in the control group of mimickers including soft tissue chondromas. We propose the name of Acral FibroChondroMyxoid Tumors for this new entity.

Supplementary information The online version of this article (https://doi.org/10.1038/s41379-020-0493-4) contains supplementary material, which is available to authorized users.

✉ Corinne Bouvier
Corinne.BOUVIER2@ap-hm.fr

1 Aix Marseille Univ, INSERM, MMG, APHM, CHU Timone, Department of Pathology, Marseille, France

2 Institut Bergonié, Department of Pathology, Université de Bordeaux, Talence, Bordeaux, France

3 Department of Pathology, CHR, Lille, France

4 Department of Pathology, Cochin hospital, Paris, France

5 Department of Bioinformatics, Institut Bergonié, Bordeaux, France

6 IUCT Oncopole, Toulouse, France

7 Department of Pathology, hôpital René-Huguenin, 35, rue Dailly, 92210 Saint-Cloud, France

8 Univ Lyon, Université Claude Bernard Lyon 1, CNRS 5286, INSERM U1052, Cancer Research Center of Lyon, Lyon, France

9 Department of Pathology, CHRU Nancy, Nancy, France

10 INSERM U1218 ACTION, Institut Bergonié, Université de Bordeaux, Talence, Bordeaux, France

11 Department of Pathology, CHRU Tours, Université de Tours, Tours, France

Introduction

In acral sites, most matrix-rich mesenchymal neoplasms are either chondromas of the soft tissues or acral fibromyxomas. However, it can be difficult to determine the nature of the stroma on microscopy, owing to the multiple aspects it may display, from complete cartilage foci to myxoid or myxohyaline. Immunohistochemistry (IHC) is of limited help: the expression of S100 and Sox9 may confirm true cartilaginous differentiation but these markers lack both sensitivity and specificity. Therefore the diagnosis of lesions associated with cartilaginous or chondromyxoid stroma can be difficult. The advent of next-generation sequencing has enabled the identification of novel recurrent gene fusions that have made a decisive contribution to redefining the classification of many previously unclassified mesenchymal tumors, with the recent example of *FN1* rearrangements in chondromas of the soft tissue to name but a few [1]. Over the past few years, we have encountered in our consultation files several acral soft tissue neoplasms associated with an abundant chondromyxoid matrix, which did not fit any consensual diagnostic category. The characterization by RNA-sequencing of these lesions led to the identification of a recurrent *THBS1-ADGRF5* gene fusion present in all cases

of this series, which prompted us to review the histopathological and clinical features of this new entity we refer to as "Acral FibroChondroMyxoid Tumors (AFCMT)" due to their distinctive morphology.

Materials and methods

Material

All cases were retrieved from the consultation files of four of the authors (CB, FLL, MN, GDP). For conventional microscopy, paraffin blocks were cut into 4 µm thick sections and stained with hematoxylin, phloxin and saffron (HPS), and in three cases with Alcian Blue. Control cases were retrieved from the archives of the soft tissue and bone sarcoma pathology review network (NETSARC+) from participating institutions, including acral fibromyxomas and soft tissue chondromas (STC). All cases were recorded in the national sarcoma pathology RREPS and RESOS databases, approved by the National Committee for the Protection of Personal Data (CNIL, n°910390), in compliance with ethics principles of the charter of Helsinki. Clinical information including follow-up were extracted from the medical records.

Immunohistochemistry

IHC was performed on a Ventana BenchMark XT or ULTRA autostainer (Ventana Medical System Inc., Tucson, AZ). The following antibodies were used: smooth muscle actin alpha (clone 1A4, prediluted; Microm), CD34 (clone QBend10, prediluted; Roche), EMA (clone E29, 1:500; Dako), S100 protein (polyclonal, 1:400; DBS), Ki67 (clone MIB-1, 1:100; Dako), Sox9 (polyclonal, 1:2000; Millipore), Sox10 (clone EP 268), 1:200; Epitomics), ERG (clone EP 111, 1:200; BioSB), AE1/AE3 (clone PCK 26, prediluted; Roche), p63 (clone 4A4, prediluted; Roche), ADGRF5 (polyclonal, ab111169, abcam).

Total RNA extraction

Total RNA was extracted from formalin-fixed paraffin-embedded (FFPE) tissues using TRIzol reagent (Invitrogen). RNA quality was assessed by Eukaryote Total RNA Nano Assay (Agilent, cat. No. 5067-1511) and DV200 was determined. RNA was stored at −80 °C.

RNA sequencing

Libraries were prepared with 100 ng of total RNA using TruSeq RNA Access Library Prep Kit (Illumina, San Diego, USA). Libraries were pooled by groups of 12 samples. Paired-end sequencing was performed using the NextSeq 500/550 High Output V2 kit (150 cycles) on Illumina NextSeq 500 platform (Illumina, San Diego, CA). The read length was 75 bp.

Sequencing data (average of 65 million reads per sample) were aligned with STAR on GRCh 38 reference genome. The fusion transcripts were calledwith STAR-Fusion, FusionMap, FusionCatcher, ERICSCRIPT and TopHat-fusion and validated if present in the fusion list of at least two algorithms. To perform the clustering analysis, gene expression values were extracted using the Kallisto v0.42.5 tool with GENECODE release 23 genome annotation based on GRCh38 genome reference. Kallisto TPM expression values were transformed in log2(TPM+2) and all samples were normalized together using the quantile method from the R limma package within R (version 3.1.1) environment. Clustering was performed with the R package Cluster v2.0.3 ConsensusClusterPlus v 1.46(12) using 1000 permutations of 80% of both samples and genes. Agnes was used as the clustering algorithm with Pearson correlation distance and Ward's clustering method. Expression analysis were performed with a Welsh *t*-test. The transcription factors of interest were selected with the following criteria: a fold change increase beyond or equal to 10 with raw p-values above or equal to 10-5 and protein coding [2–5].

Reverse transcription polymerase chain reaction (RT-PCR)

An aliquot of the RNA extracted from FFPE tissue was used to confirm the novel fusion transcripts identified. One microgram of total RNA was reverse transcribed in cDNA by High Capacity cDNA Reverse Transcription Kit with RNase Inhibitor (Invitrogen, cat. No. 4374966). PCR was performed using the AmpliTaq Gold™ DNAPolymerase kit (Applied Biosystems™, cat. No. 4311806) on 50 ng of cDNA with the following primers: THBS1_FWD: 5′ GGTGGTAGACTAGGGTTGTTT 3′ and GPR116_REV: 5′ CCTCAGAAACAGAAATTGGGTC 3′. Touchdown 60 °C program was used (TD 60 °C; two cycles at 60 °C, followed by two cycles at 59 °C, two cycles at 58 °C, three cycles at 57 °C, three cycles at 56 °C, four cycles at 55 °C, four cycles at 54 °C, five cycles at 53 °C, and finally 10 cycles at 52 °C). PCR products were then purified using Illustra ExoProStar™ PCR Purification Kit (GE Healthcare, cat. No.US77702), and sequencing reactions were performed with the Big Dye Terminator V1.1 Kit (Applied Biosystems, cat. No. 4337450). After purification with the Big Dye XTerminator Purification Kit (Applied Biosystems,cat. No. 4376486), the samples were sequenced on a 3130xl Genetic Analyzer (Applied Biosystems).

Results

Clinical findings

Patients' age at diagnosis ranged from 20 to 64 years (median: 42). No pediatric case was observed (Table 1). There was a male predominance (male to female ratio: 7/3). Tumors were located in the hands ($n = 7/10$) and feet ($n = 3/10$), affecting mostly the fingers and phalanges but also the metacarpophalangeal joint in two cases. The size of lesions was not available since tumors were resected in fragments and no prior radiological work-up was available in most cases. Tumors presented as painless nodule of the extremity in seven cases but were painful in a minority of cases ($n = 3/10$, cases no. 4, 6, 9). Five tumors invaded the adjacent bone. All tumors were treated with marginal resection without the need to perform digital amputation. The series included eight primary and two recurrent tumors. No recurrence was seen among the 8 primary cases (median clinical follow-up = 17.5 months, range: 3–41 months).

Pathological findings

Ten cases were reviewed included eight primary and two recurrences (Figs. 1 and 2). The initial diagnosis was chondroma in four cases, superficial acral fibromyxoma (SAFM) in two cases (one of which was notified as displaying cartilaginous metaplasia), myoepithelioma in two cases and one case each had been labeled as chondromyxoid fibroma, and unclassified benign myxoid tumor. All but one tumor displayed nodular or multinodular growth (Fig. 1a, b), delineated by fibrous bands ($n = 9/10$) (Fig. 1c). Only one case was associated with a more diffuse growth pattern. Numerous small vessels were present within the fibrous septa (Fig. 1d). No inflammation was seen. Tumor cells were embedded in an abundant variable stroma which contained fibrous, chondroid, and myxoid areas (Fig. 2a, b). The myxoid matrix diffusely stained with alcian blue (Fig. 2d). The cellular areas were in abrupt transition with the hypocellular and fibrous areas sometimes containing small cystic-like changes ($n = 2/10$). More rarely, the stroma displayed foci of calcifications and foci of ischemic necrosis in one case each (Fig. 2e). The neoplastic cells were either arranged in ill-defined groups (Fig. 2d) or formed small clusters (Fig. 2a, b) and rows (Fig. 2c). The cells were focally embedded within lacunar spaces, hinting at a cartilaginous differentiation (Fig. 2c). The neoplastic cells had small round, ovoid or reniform nuclei with inconspicuous nucleoli. The nuclei displayed longitudinal grooves reminiscent of chondroblasts in five cases (Fig. 2c). Binucleation was also occasionally seen. The cells had a limited amount of cytoplasm in most cases while it was more abundant with a plamacytoid appearance in two cases,

Table 1 Clinicopathological and Molecular findings.

ID	Initial diagnosis	Age/gender	Location	Fusion type	Sample type	Bone involvement	Treatment	Follow-up (months)
Case 1	Chondroma or chondromyxoid fibroma	20/F	Foot (left T3)	*THBS1*(e21)-*ADGRF5*(e12)	Recurrence	Yes	Surgery	NA
Case 2		48/M	Hand (left P1)	*THBS1*(e21)-*ADGRF5*(e12)	Primary	No	Surgery	NED (14)
Case 3	Chondromyxoid fibroma	36/M	Foot (left T2 P3)	*THBS1*(e21)-*ADGRF5*(e12)	Primary	Yes	Surgery	NED (42)
Case 4	Acral fibromyxoma	37/M	Hand (left D2 Metacarpophalangeal joint)	*THBS1*(e21)-*ADGRF5*(e12)	Primary	Yes	Surgery	NED (21)
Case 5	Soft-tissue chondroma	64/M	Hand (right D3)	*THBS1*(e21)-*ADGRF5*(e12)	Primary	No	Surgery	NED (13)
Case 6	Soft-tissue chondroma	45/F	Hand (D3 P1)	*THBS1*(e21)-*ADGRF5*(e12)	Primary	No	Surgery	NED (12)
Case 7	Soft-tissue chondroma	58/M	Capsula of right metacarpophalangeal joint of D4	*THBS1*(e21)-*ADGRF5*(e9)	Primary	Yes	Surgery	NED (26)
Case 8	Acral fibromyxoma	50/M	Foot (right T2)	*THBS1*(e21)-*ADGRF5*(e12)	Primary	No	Surgery	NED (32)
Case 9	Myoepithelioma	24/M	Hand (D2 P3)	*THBS1*(e21)-*ADGRF5*(e12)	Primary	Yes	Surgery	NED (3)
Case 10	Myoepithelioma	37/F	Hand (D3 P3)	*THBS1*(e21)-*ADGRF5*(e12)	Recurrence	No	Surgery	NED (14)

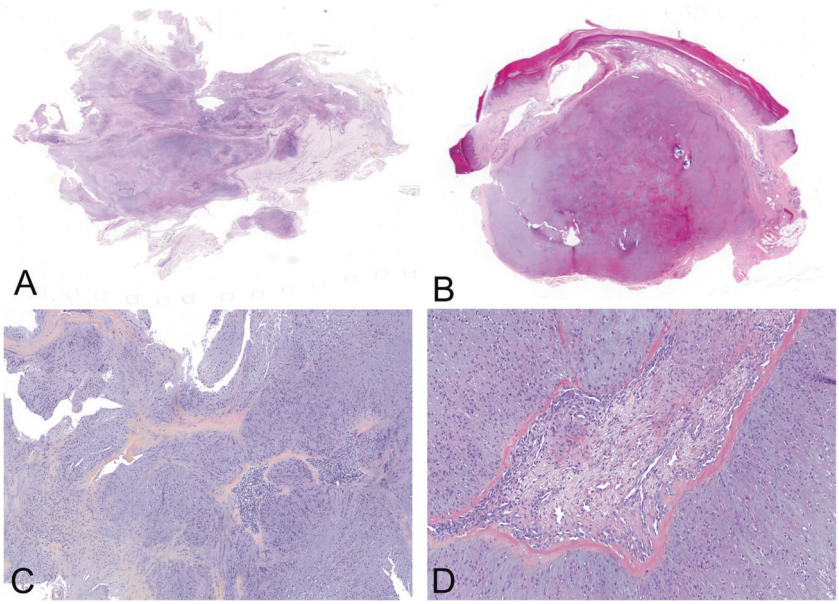

Fig. 1 AFCMT displays a multinodular, lobulated silhouette, with an abundant myxoid to chondroid matrix. Cases may appear poorly delineated (**a**) or as a well-circumscribed nodule (**b**). In AFCMT, lobules are composed of an abundant chondroid to myxoid matrix, delineated by fibro-vascular septa imparting a lobular appearance. The collagen delineating the periphery of the lobule is often thick and hyaline (**c**). Within lobules, neoplastic cells are bland, with a round cytology, eosinophilic cytoplasm and arranged in columns or small clusters. Septa display a characteristic hypervascularization. Similar epithelioid or spindle cells can also be identified within the septa or around vessels (**d**).

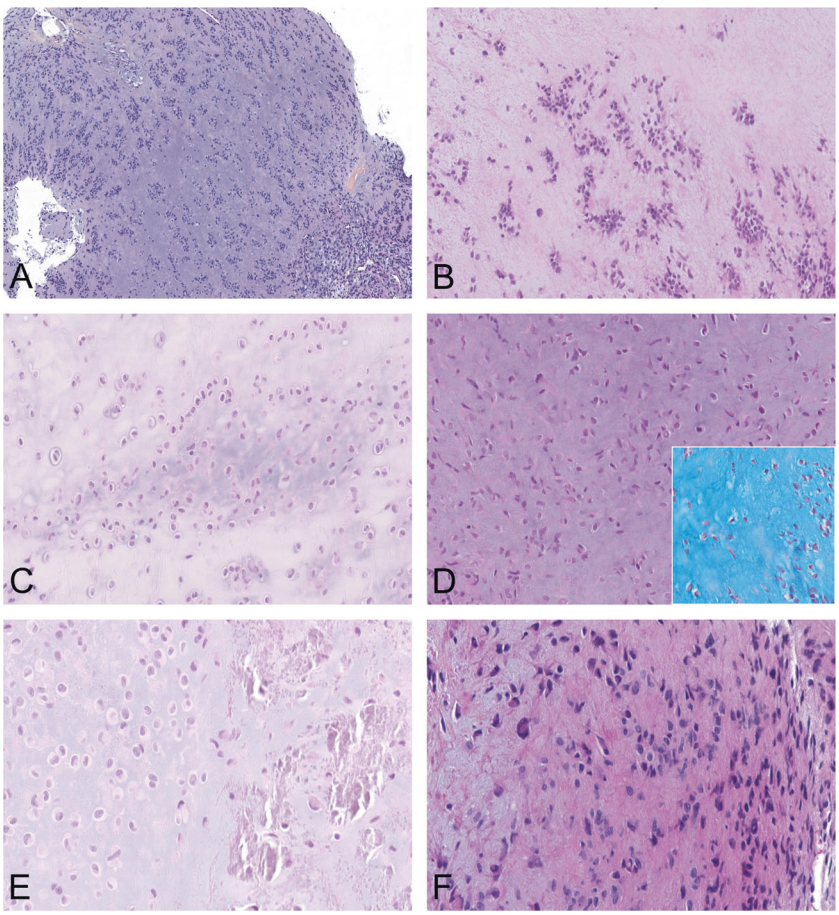

Fig. 2 Micoscopic features. Low-power examination reveals arrangement of neoplastic cells in small groups or clusters dispersed within the myxoid matrix (**a**, **b**). Neoplastic cells display an epithelioid cytology, with oval or reniform nuclei, imparting a chondroblast-like appearance; some of them are embedded in lacunae surrounded by an abundant extracellular matrix, imparting a chondroid appearance. Outside clusters, cells may also follow a linear or a haphazard arrangement (**c**). In myxoid areas (with intense staining with Alcian Blue), cells endorse a more spindled morphology and lacunae are less readily identified (**d**). Rarely, calcifications can be identified within the matrix (**e**). A single case displayed enlarged and slightly hyperchromatic nuclei imparting a pleomorphic cytology but without mitotic activity (**f**).

or elongated giving a spindle cell look to the proliferation in three cases. Slight variations in size and shape of the nuclei were present without overt pleomorphism, but in one case the nuclei were focally significantly enlarged and hyperchromatic (Fig. 2f). No mitotic activity was seen.

Immunohistochemical findings

Tumor cells consistently expressed CD34 (10/10), ERG (9/10) and SOX9 (7/10) (Table 2, Fig. 3). CD34 stained both the neoplastic cells and the adjacent regional matrix in all cases with reinforcement at the periphery of the lobules. ERG stained the nuclei of the tumor cells either diffusely ($n = 5/9$) or focally ($n = 4/9$). The staining pattern was weak as compared with the endothelial cells. SOX9 expression was diffuse in two cases, focal in five cases. S100 protein displayed a faint and focal staining in five cases. No expression of AE1/AE3, EMA, smooth muscle actin alpha or SOX10 was observed. P63 was focally expressed in two cases. The proliferation index assessed by Ki67 staining was below 5% in all cases. No significant staining was identified using an antibody against ADGRF5 protein.

Molecular findings

THBS1-ADGRF5 fusions were identified by whole RNA-sequencing on FFPE material in 8 cases and by RT-PCR in two cases (Table 3, Fig. 4). The presence of the fusion was

Table 2 Immunohistochemical findings.

	CD34 (%)	ERG (%)	SOX9 (%)	PS100 (%)	P63 (%)	EMA (%)	AE1/AE3 (%)	SMA (%)	SOX10 (%)	Ki67 (%)
Case 1	+F	+D	+D	+F	–	–	–	–	–	<5
Case 2	+F	–	+F	+F	–	–	–	–	NA	NA
Case 3	+F	+F	+F	–	–	–	–	–	–	<5
Case 4	+F	+F	+F	+F	–	–	–	–	–	<5
Case 5	+F	+D	+F	–	–	–	–	–	–	<5
Case 6	+D	+F	–	+F	–	–	–	–	–	<5
Case 7	+F	+D	+D	+F	+F	–	–	–	–	<5
Case 8	+F	+D	+F	–	–	+F	–	–	–	<5
Case 9	+F	+F	–	–	–	–	–	–	–	<5
Case 10	+D	+F	–	–	+F	–	–	–	–	<5
Positive cases	10 (100)	9 (90)	7 (70)	5 (50)	2 (20)	1 (10)	0 (0)	0 (0)	0 (0)	<5
Focal	8 (80)	5 (50)	5 (50)	5 (50)	2 (20)	1 (10)	0 (0)	0 (0)	0 (0)	
Diffuse	2 (20)	4 (40)	2 (20)	0 (0)	0 (0)	0 (0)	0 (0)	0 (0)	0 (0)	

F focal, *D* diffuse, *NA* not available.

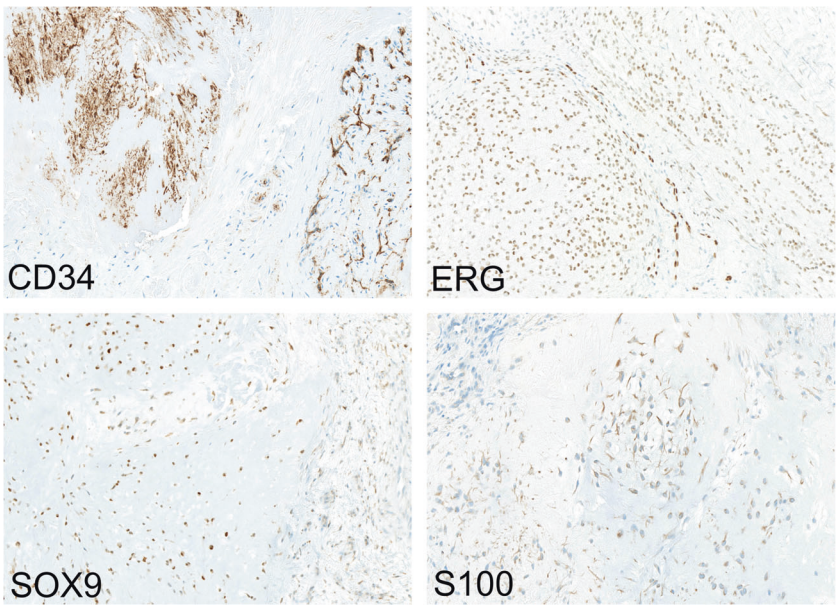

Fig. 3 Classic pattern of immunostains is characterized by a focal and patchy expression of S100 protein, CD34 staining of neoplastic cells and extracellular matrix, diffuse nuclear expression of SOX9 and ERG. ERG intensity is decreased in comparison with endothelium.

confirmed by RT-PCR in all cases. *THBS1-ADGRF5* fusion involved exon 21 of *THBS1* and exon 12 of *ADGRF5* in all but one case. The fusion involved exon 9 of *ADGRF5* in one case.

Mutational analysis revealed the presence of *ATM* mutation in 2 cases ($n = 2/8$), *NOTCH2* ($n = 1/8$) and *KDR* ($n = 1/8$). No tumor harbored *IDH1/2* mutation.

We tested the specificity of *THBS1-ADGRF5* fusion in a control cohort of acral tumors including 11 SAFM, three myoepitheliomas, three STCs of the extremities, one calcifying aponeurotic fibroma and one perineurioma. The fusion transcript was not detected by RT-PCR and RNA-sequencing in any of the control cases (Supplementary Table 1).

The expression profiles of five tumors associated with *THBS1-ADGRF5* were compared to those of nine acral tumors including five superficial acral fibromyxomas, one perineurioma, one calcifying aponeurotic fibroma, and one myoepithelioma. On unsupervised clustering analysis, all

Table 3 Molecular data.

ID serie	RT-PCR THBS1-ADGRF5	RNA-seq	Mutation analysis
Case 1	Positive	*THBS1*(e21)-*ADGRF5*(e12)	NA
Case 2	Positive	*THBS1*(e21)-*ADGRF5*(e12)	NOTCH2:NM_001200001:exon22:c.T3625G:p.F1209V (COSMIC) ATM:NM_000051:exon9:c.T1229C:p.V410A (COSMIC)
Case 3	Positive	*THBS1*(e21)-*ADGRF5*(e12)	WT
Case 4	Positive	*THBS1*(e21)-*ADGRF5*(e12)	KDR:NM_002253:exon16:c.C2312T:p.T771M (COSMIC)
Case 5	Positive	*THBS1*(e21)-*ADGRF5*(e12)	ATM:NM_000051:exon9:c.T1229C:p.V410A (COSMIC)
Case 6	Positive	*THBS1*(e21)-*ADGRF5*(e12)	WT
Case 7	Positive	*THBS1*(e21)-*ADGRF5*(e9)	WT
Case 8	Positive	NA	NA
Case 9	Positive	NA	NA
Case 10	Positive	*THBS1*(e21)-*ADGRF5*(e12)	WT

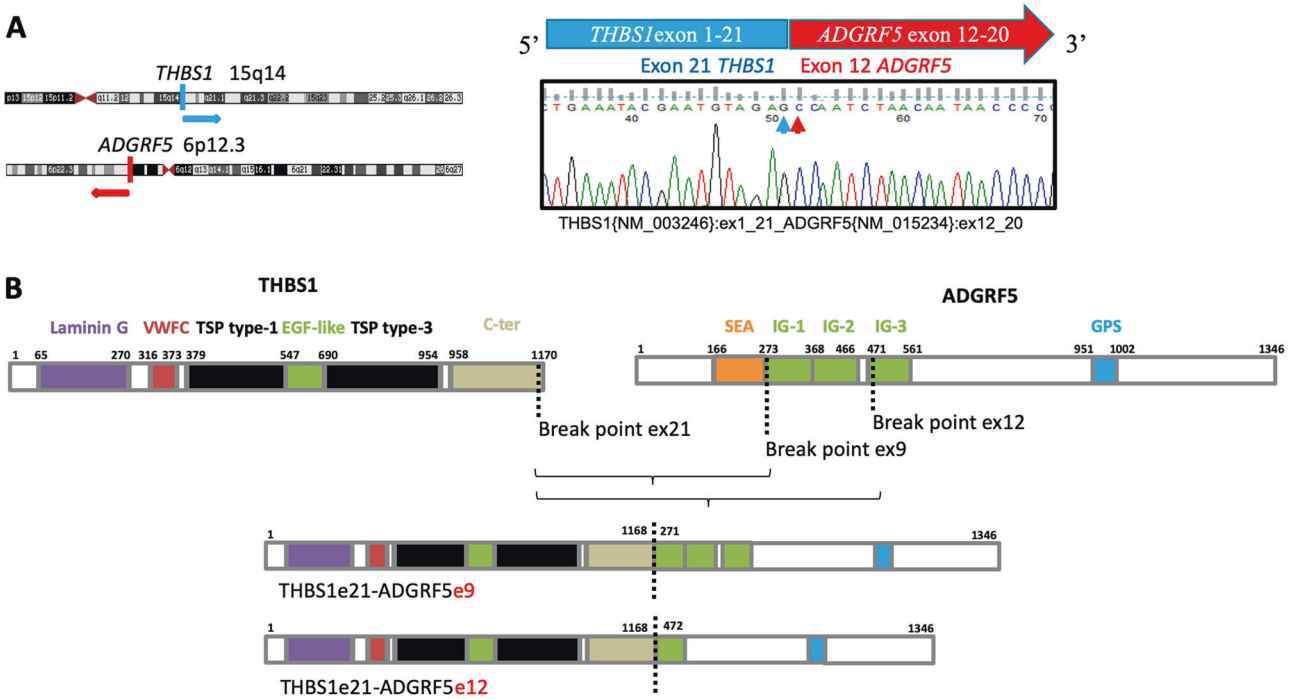

Fig. 4 Structure and breakpoints of *THBS1-ADGRF5* fusions. The left panel shows the location of *THBS1* and *ADGRF5* loci and orientation of each genes. The right panel illustrates the cDNA sequence of the most common fusion, involving exon 21 of *THBS1* and exon 12 of *ADGRF5*. Arrows indicate the break-point for each gene (**a**). Schematic representation of the structure of the respective proteins. The dotted lines indicate the location of the breakpoints in the domain and the structure of the chimeric THBS1-ADGRF5 protein is shown below, with the theoretically retained domains (**b**). GPS GPCR proteolytic site motif, Ig-like immunoglobulin-like domain, VWFD Von Willebrand Factor domain, EGF epidermal growth factor.

but one *THBS1-ADGRF5* clustered tightly together (Supplementary Fig. 1). The single case which clustered differently from the main cohort was classified among two cases of acral fibromyxomas. On expression analysis with a Welsh *t*-test, the two most differentially expressed genes in *THBS1-ADGRF5* tumors as opposed to the control group were *ADGRF5* and the natriuretic peptide receptor 3 (NRP3) (Supplementary Table 2). By IHC, no overexpression of ADGRF5 was observed.

Discussion

Most acral tumors with an abundant matrix correspond to chondroma, myoepithelioma and acral fibromyxoma. Due to the absence of specific biomarkers and the difficulty of assessing the exact nature of the matrix, these lesions can be difficult to classify with certainty.

We describe herein a distinctive clinicopathological entity that we have named acral fibrochondromyxoid tumors (AFCMT). This tumor occurs electively in acral sites and is associated with an abundant stroma displaying fibrous, chondroid and myxoid areas. AFCMT are associated with recurrent *THBS1-ADGRF5* fusions. They affect adult patients, especially male, and develop mainly in the soft tissue although they may infiltrate the underlying bone. Most cases of AFCMT are located near the phalanges of fingers and toes and present clinically as a small multinodular non-encapsulated mass. Histologically, AFCMT have a multinodular growth pattern composed of a proliferation of small monotonous ovoid to spindle cells, sometimes associated with features reminiscent of chondrocytic or chondroblastic differentiation such as coffee bean nuclei or small lacunar spaces. AFCMT are associated with an abundant fibrous or chondromyxoid stroma which is reminiscent of cartilaginous differentiation, accounting for the previous misclassification of these lesions as chondromas or myoepitheliomas. AFCMT consistently express CD34 (100%), ERG (90%), and Sox9 (70%). The coexpression of CD34 and S100 protein is a feature of normal fibrocartilage [6, 7] and ERG is usually expressed by cartilaginous neoplasms [8]. Consequently, both histological and immunohistochemical features hint at a partial cartilaginous differentiation in AFCMT.

AFCMT are not associated with aggressive morphological or clinical features, supporting their benign nature, though further studies with longer follow-up are required to confirm their indolent behavior.

Their specific *THBS1-ADGFR5* fusion involves *THROMBOSPONDIN-1* (*THBS1*) as the 5′ partner which encodes a member of the family of non-collagenous matrix glycoproteins of the extracellular matrix (ECM) [9]. These proteins interact with growth factors, ECM proteins and cell-surface receptors. They also control the organization of the ECM through the regulation of post-translational modifications of fibrillar collagens [10, 11]. *THBS1* is also involved in the regulation of platelet adhesion and inhibits angiogenesis in physiologic and tumor conditions [12]. It has been shown to mediate the antiangiogenic effect of trabectedin [13]. Structurally, *THBS1* contains a laminin G domain involved in the interaction with heparin, one type C Von-Willebrand Factor domain which is a collagen binding region and three TSP type I, three TSP type II (EGF-like) and seven TSP type III domains (Fig. 4b).

THBS1 has been previously identified as a 5′ fusion partner of *ALK* in inflammatory myofibroblastic tumors (IMT) of the uterus [14] leading to ALK overexpression. Likewise, this fusion leads to ADGFR5 upregulation and this hypothesis is supported by the expression data (Supplementary Table 2). Interestingly, the breakpoints occurred within exon 4 in IMT and exon 21 in this series. Therefore the protein is entirely conserved in AFCMT. As a key organizer of the ECM, THBS1 involvement may most probably account for the abundant matrix observed in AFCMT.

3′ fusion partner of this fusion involves *ADGRF5* (also known as *GPR116*) located in 6p12.3, which encodes an orphan transmembrane G-protein-coupled receptor part of the family of G-protein-coupled receptors. The protein is involved in the regulation of vasculature development [15] especially in the kidney [16] and in the homeostasis of lung surfactant [17]. Structurally, ADGRF5 protein contains a SEA domain, involved in O-glycosylation, Immunoglobulin-like (Ig-like) domains involved in cell-cell recognition, interaction with cell-surface receptors and with immune cells, one GPS motif (GPCR proteolytic site), which is involved in the cleavage of the protein, and the C-terminal region which contains the seven transmembrane domains. The breakpoints were located before exon 12, therefore preserving the SEA box (serving as an auto-proteolytic cleavage domain) and immunoglobulin-like repeats motifs that may have immunologic functions [18]. The sequences encoding the transmembrane domains of the protein which were notably conserved as the genomic breakpoints were located in 5′, therefore preserving the transmembranous location of the protein (Fig. 4b).

At transcriptional level, all tumors displayed a major upregulation of ADGRF5 transcript but this finding was not confirmed at protein level by IHC (data not shown). *ADGRF5* upregulation has been previously shown to correlate with tumor progression and metastasis in breast [19] and colorectal carcinomas [20] by promoting cell motility and the formation of lamellipodia [19]. but the mechanism underlying the upregulation in these tumors were not studied. The clinical follow-up of our series does not suggest that AFCMT have a malignant potential.

AFCMTs are associated with a distinct stroma that may give rise to several differential diagnoses including mainly

STC, synovial chondromatosis (SC), myoepithelial neoplasms, and to a lesser extent SAFM.

STC represent the main differential diagnosis. Four cases of this series had indeed been classified as such. STC share the same clinical presentation as AFCMT affecting middle-aged adults with common location in the extremities. Nonetheless STC rarely invades bone though it can cause compression or erosion [21], contrasting with the common occurrence of bone infiltration in half of the cases in this series. Both tumors can relapse if incompletely resected. On microscopy, STC are primarily made of lobules of mature hyaline cartilage, distinct from the immature chondroid and myxoid stroma displayed by AFCMT. By contrast, in AFCMT the lobules are delineated by a rich fibrovascular network. STC are associated in half of cases with *FN1* fusions [1]. The morphological differences between AFCMT and STC may be related to the distinct consequences of the respective fusions involved in these lesions.

Likewise, SC can occasionally affect small joints of hands and feet, referred to as 'Tenosynovial chondromatosis' when occurring in extra-articular locations. SC are predominantly associated with mature cartilage formation and focally the synovia is seen. SC are associated in half of cases with *FN1-ACVR2A* fusions [1].

Myoepithelial neoplasms also come within the differential diagnosis. Initially, two cases of AFCMTs were diagnosed as myoepitheliomas. Myoepitheliomas are also associated with multinodular growth and variable myxoid, hyalinized and chondroid stroma. They typically coexpress SOX10 and/or S100 protein and epithelial antigens (cytokeratin and/or EMA). Both Sox10 and epithelial markers are consistently negative in AFCMT. Furthermore they are associated with *EWSR1* or *FUS* fusions in roughly half of cases [22, 23].

SAFM represent another important differential in the digits. They also affect male adults [24]. Nonetheless, SAFM typically involve the subungueal region and are morphologically distinct, made of hypocellular myxoid nodules containing bland-looking fibroblast-like cells loosely arranged in a storiform pattern. Cartilaginous metaplasia has been reported in a subset of SAFM [24, 25]. Rb1 loss is frequent in SAFM [26].

In addition, chondromyxoid fibromas (CMF) are ubiquitous cartilaginous neoplasms of bone. Similarly to AFCMT, CMF exhibits a lobulated matrix combining a variable combination of chondroid, myxoid, and fibrous areas. The cellularity is also variable with hypocellular central areas and peripheral reinforced cellularity. In contrast to AFCMT, CMF may contain coarse calcifications and display 'stellate' or sometimes tumor cells along with osteoclasts. Both AFCMT and CMF express ERG, S100 and SOX9 but CMF are usually negative for CD34 [8, 27]. Recently, recurrent GRM1 fusions have been identified in CMF [28].

Calcifying aponeurotic fibromas (CAF) are lesions that contain chondroid foci, therefore coming within the differential with AFCMT. CAF affect children and young adults, developing in palms and soles. Albeit infiltrative, CAF does not invade bone. Histologically, they are made of spindle cell proliferation reminiscent of fibromatosis which is admixed with small round or ovoid foci of calcifications. Calcification and chondroid matrix are usually seen in the central part of the lesion. This zonal organization is not seen in AFCMT. CAF harbor *FN1-EGF* gene fusions [29].

Ectomesenchymal chondromyxoid tumors share similar morphological features with AFCMT but they have been described exclusively in the tongue and harbor a distinctive RREB1-MKL2 fusion [30]. Albeit exceptional in acral location, extra-axial extraosseous chordoma [31, 32] and extraskeletal myxoid chondrosarcoma [33] may also be included in the differential diagnosis.

In summary, we report the clinicopathological and genetic features of a new distinctive subtype of acral soft tissue tumors. AFCMT is characterized by a lobular pattern with marked fibrovascular septa, a chondromyxoid stroma, round or spindle bland cells and expression of CD34, SOX9, and ERG. The main differential diagnosis is STC. AFCMT are associated with recurrent *THBS1-ADGFR5* fusions and follow a benign course although local recurrence is possible. These tumors further add to the spectrum of neoplasms associated with an abundant matrix and harboring recurrent fusions, such as STCs, SC and calcifying aponeurotic fibroma. Our findings contribute to better delineation of these partially overlapping entities.

Acknowledgements This work was supported by a grant from the charity *Au Fil d'Oriane*. We are grateful to pathologists and clinicians for sharing cases and follow-up information: G. Barnéon (MEDIPATH, Grabels, France), C. Charon-Barra (Centre Georges François Leclerc, Dijon, France), O. Laghmari (Institut d'histopathologie, Nantes, France), M. Paoli-Labbe (Centre de Pathologie Bastiais, France), A. Rousseau (Biopath Aquitaine, Le Haillan), AV Decouvelaere (Cypath, Villeurbanne, France),Ch. Delfour (Hôpital G. De Chauliac, Montpellier, France). The authors are grateful to V. Velasco for her excellent technical assistance.

Compliance with ethical standards

Conflict of interest The authors declare that they have no conflict of interest.

Publisher's note Springer Nature remains neutral with regard to jurisdictional claims in published maps and institutional affiliations.

References

1. Amary F, Perez-Casanova L, Ye H, Cottone L, Strobl AC, Cool P, et al. Synovial chondromatosis and soft tissue chondroma: extraosseous cartilaginous tumor defined by FN1 gene rearrangement. Mod Pathol. 2019. https://doi.org/10.1038/s41379-019-0315-8.

2. Bray NL, Pimentel H, Melsted P, Pachter L. Near-optimal probabilistic RNA-seq quantification. Nat Biotechnol. 2016;34:525–7.
3. Ge H, Liu K, Juan T, Fang F, Newman M, Hoeck W. FusionMap: detecting fusion genes from next-generation sequencing data at base-pair resolution. Bioinformatics. 2011;27:1922–8.
4. Trapnell C, Roberts A, Goff L, Pertea G, Kim D, Kelley DR, et al. Differential gene and transcript expression analysis of RNA-seq experiments with TopHat and Cufflinks. Nat Protoc. 2012;7:562–78.
5. Le Loarer F, Watson S, Pierron G, De Montpreville VT, ballet S, Firmin N, et al. SMARCA4 inactivation defines a group of undifferentiated thoracic malignancies transcriptionally related to BAF-deficient sarcomas. Nat Genet. 2015;47:1200–5.
6. Zamecnik M, Michal M. Nuchal fibrocartilaginous pseudotumor: immunohistochemical and ultrastructural study of two cases. Pathol Int. 2001;51:723–8.
7. Declercq HA, Forsyth RG, Verbruggen A, Verdonk R, Cornelissen JJ, Verdonk PC, et al. CD34 and SMA expression of superficial zone cells in the normal and pathological human meniscus. J Orthop Res. 2012;30:800–8.
8. Shon W, Folpe AL, Fritchie KJ. ERG expression in chondrogenic bone and soft tissue tumours. J Clin Pathol. 2015;68:125–9.
9. Adams JC, Lawler J. The thrombospondins. Cold Spring Harb Perspect Biol. 2011;3:a009712.
10. Rosini S, Pugh N, Bonna AM, Hulmes DJS, Farndale RW, Adams JC. Thrombospondin-1 promotes matrix homeostasis by interacting with collagen and lysyl oxidase precursors and collagen cross-linking sites. Sci Signal. 2018;11. https://doi.org/10.1126/scisignal.aar2566.
11. DiCesare PE, Mörgelin M, Mann K, Paulsson M. Cartilage oligomeric matrix protein and thrombospondin 1. Purification from articular cartilage, electron microscopic structure, and chondrocyte binding. Eur J Biochem. 1994;223:927–37.
12. Potikyan G, Savene RO, Gaulden JM, France KA, Zhou Z, Kleinerman ES, et al. EWS/FLI1 regulates tumor angiogenesis in Ewing's sarcoma via suppression of thrombospondins. Cancer Res. 2007;67:6675–84.
13. Antiangiogenic activity of trabectedin in myxoid liposarcoma: involvement of host TIMP-1 and TIMP-2 and tumor thrombospondin-1.—PubMed—NCBI. https://www.ncbi.nlm.nih.gov/pubmed/?term=24917554. Accessed 4 Oct 2019.
14. Haimes JD, Stewart CJR, Kudlow BA, Culver BP, Mong B, Koay E, et al. Uterine inflammatory myofibroblastic tumors frequently harbor ALK fusions with IGFBP5 and THBS1. Am J Surg Pathol. 2017;41:773–80.
15. Prömel S, Waller-Evans H, Dixon J, Zahn D, Colledge WH, Doran J, et al. Characterization and functional study of a cluster of four highly conserved orphan adhesion-GPCR in mouse. Dev Dyn. 2012;241:1591–602.
16. Lu S, Liu S, Wietelmann A, Kojonazarov B, Atzberger A, Tang C, et al. Developmental vascular remodeling defects and postnatal kidney failure in mice lacking Gpr116 (Adgrf5) and Eltd1 (Adgrl4). PLoS ONE. 2017;12:e0183166.
17. Yang MY, Hilton MB, Seaman S, Haines DC, Nagashima K, Burks, et al. Essential regulation of lung surfactant homeostasis by the orphan G protein-coupled receptor GPR116. Cell Rep. 2013;3:1457–64.
18. Fredriksson R, Lagerström MC, Höglund PJ, Schiöth HB, et al. Novel human G protein-coupled receptors with long N-terminals containing GPS domains and Ser/Thr-rich regions. FEBS Lett. 2002;531:407–14.
19. Tang X, Jin R, Qu G, Wang X, Li Z, Yuan Z, et al. GPR116, an adhesion G-protein-coupled receptor, promotes breast cancer metastasis via the Gαq-p63RhoGEF-Rho GTPase pathway. Cancer Res. 2013;73:6206–18.
20. Yang L, Lin X-L, Liang W, Fu SW, Lin WF, Tian XQ, et al. High expression of GPR116 indicates poor survival outcome and promotes tumor progression in colorectal carcinoma. Oncotarget. 2017;8:47943–56.
21. Cho SH, Horvai A. chondro-osseous lesions of soft tissue. Surg Pathol. 2015;8:419–44.
22. Agaram NP, Chen H-W, Zhang L, Sung YS, Panicek D, Healey JH, et al. EWSR1-PBX3: a novel gene fusion in myoepithelial tumors. Genes Chromosomes Cancer. 2015;54:63–71.
23. Antonescu CR, Zhang L, Chang N-E, Pawel BR, Travis W, Katabi N, et al. EWSR1-POU5F1 fusion in soft tissue myoepithelial tumors. A molecular analysis of sixty-six cases, including soft tissue, bone, and visceral lesions, showing common involvement of the EWSR1 gene. Genes Chromosomes Cancer. 2010;49:1114–24.
24. Hollmann TJ, Bovée JVMG, Fletcher CDM. Digital fibromyxoma (superficial acral fibromyxoma): a detailed characterization of 124 cases. Am J Surg Pathol. 2012;36:789–98.
25. Moulonguet I, Goettmann S, Zaraa I. Superficial acral fibromyxoma with cartilaginous metaplasia. Am J Dermatopathol. 2019;41:316–7.
26. Agaimy A, Michal M, Giedl J, Hadravsky L, Michal M. Superficial acral fibromyxoma: clinicopathological, immunohistochemical, and molecular study of 11 cases highlighting frequent Rb1 loss/deletions. Hum Pathol. 2017;60:192–8.
27. Nielsen GP, Keel SB, Dickersin GR, Selig MK, Bhan AK, Rosenberg AE. Chondromyxoid fibroma: a tumor showing myofibroblastic, myochondroblastic, and chondrocytic differentiation. Mod Pathol. 1999;12:514–7.
28. Nord KH, Lilljebjörn H, Vezzi F, Nilsson J, Magnusson L, Tayebwa J, et al. GRM1 is upregulated through gene fusion and promoter swapping in chondromyxoid fibroma. Nat Genet. 2014;46:474–7.
29. Puls F, Hofvander J, Magnusson L, Nilsson J, Haywood E, Sumathi VP, et al. FN1-EGF gene fusions are recurrent in calcifying aponeurotic fibroma. J Pathol. 2016;238:502–7.
30. Dickson BC, Antonescu CR, Argyris PP, Bilodeau EA, Bullock MJ, Freedman PD, et al. Ectomesenchymal chondromyxoid tumor: a neoplasm characterized by recurrent RREB1-MKL2 fusions. Am J Surg Pathol. 2018;42:1297–305.
31. Bitzer A, McCarthy EF, Morris CD. Extra-axial chordoma of the hand. J Hand Surg Am. 2017;42:933.e1–933.e5.
32. Righi A, Sbaraglia M, Gambarotti M, Cocchi S, Drago G, Casadei R, et al. Extra-axial chordoma: a clinicopathologic analysis of six cases. Virchows Arch. 2018;472:1015–20.
33. Urbini M, Astolfi A, Pantaleo MA, Serravalle S, Dei Tos AP, Picci P, et al. HSPA8 as a novel fusion partner of NRA3 in extraskeletal myxoid chondrosarcoma. Genes Chromosomes Cancer. 2017;56:582–6.